

Structure-Dependence of Kinetic and Thermodynamic Parameters in Singlet Fission Processes

Daphné Lubert-Perquel^{1†}, Anna A. Szumska², Mohammed Azzouzi², Enrico Salvadori^{3*}, Stefan Ruloff⁴, Christopher M. W. Kay^{4,5}, Jenny Nelson^{2*} and Sandrine Heutz^{1*}*

¹ London Centre for Nanotechnology and Department of Materials, Imperial College London, Prince Consort Road, London SW7 2BP, U.K.

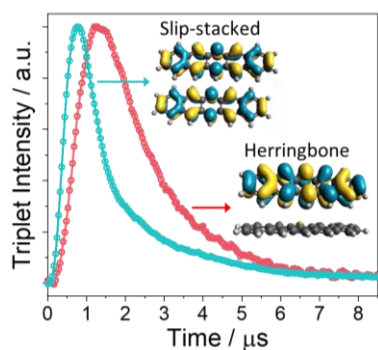
² Department of Physics, Imperial College London, Prince Consort Road, London SW7 2BP, U.K.

³ Department of Chemistry, University of Turin, Via Giuria 7, Turin 10125, Italy

⁴ Department of Chemistry, University of Saarland, 66123 Saarbrücken, Germany

⁵ London Centre for Nanotechnology, University College London, 17-19 Gordon Street, London WC1H 0AH, UK.

Singlet fission – whereby one absorbed photon generates two coupled triplet excitons – is a key process for increasing the efficiency of optoelectronic devices by overcoming the Shockley-Queisser limit. A crucial parameter is the rate of dissociation of the coupled triplets, as this limits the number of free triplets subsequently available for harvesting and ultimately the overall efficiency of the device. Here, we present an analysis of the thermodynamic and kinetic parameters for this process in parallel and herringbone dimers measured by electron paramagnetic resonance spectroscopy in co-evaporated films of pentacene in p-terphenyl. The rate of dissociation is faster for parallel dimers than for their herringbone counterparts, as is the recombination to the ground state. DFT calculations, which provide the magnitude of the electronic coupling as well as the distribution of molecular orbitals for each geometry, suggest that lower triplet coupling in the parallel dimer is the driving force for faster dissociation. Conversely, localization of the molecular orbitals and stronger triplet-triplet interaction result in slower dissociation and recombination. The identification and understanding of how intermolecular geometry promote efficient triplet dissociation provides the basis for control of triplet coupling and thereby the optimization of one important parameter of device performance.



KEYWORDS. Pentacene, molecular semiconductor, EPR spectroscopy, triplet, quintet.

Distance and relative orientation between chromophores dictate the nature and strength of their electronic coupling influencing their behaviour and usefulness in technological applications. Photosynthetic complexes, where the protein scaffold holds chlorophyll and carotenoid chromophores in precisely defined positions, provide striking examples of this. For instance, the precise arrangement of bacteriochlorophylls in the LH2 complex considerably redshifts the absorption wavelength of the complex compared to the monomer.^{1,2}

In common organic photovoltaics, where photosynthetic light conversion reactions are mimicked, the active components are distributed within amorphous or polycrystalline structures and the overall efficiency is a weighted average over all possible distances and orientations. Singlet fission (SF) - a mechanism by which one singlet exciton splits into two triplet excitons - has gained prominence as a viable pathway for exceeding the Shockley-Queisser limit, the theoretical maximum efficiency of a solar cell. SF could improve the efficiency of a hybrid organic-inorganic photovoltaic structure, whereby an organic layer on top of an inorganic solar cell harvests high-energy photons and supplies two lower energy excitations to the underlying inorganic layer, typically a crystalline silicon p-n junction, in which charge separation is accomplished.³⁻⁶ The SF process can be described by the equation:



where S_0 and S_1 are the ground and (first) excited singlet states, respectively; ${}^1(\text{TT})$ are the coupled triplets with singlet multiplicity produced by SF; and $\text{T} + \text{T}$ are the free triplets available after fission for harvesting. An intermediate step often labelled $(\text{T} \dots \text{T})$ but not shown here as it cannot be directly distinguished in our study, represents triplet pairs that are spatially separated so that whilst they retain spin coherence, the coupling is sufficiently weakened allowing spin mixing,

resulting in the formation of quintets⁷. Here we use the notation $^5(\text{TT})$ to denote quintets, as they are unambiguously identified using electron paramagnetic resonance (EPR) spectroscopy and can therefore be specified.⁸⁻¹⁰

Not many organic semiconductors are known to undergo SF mostly because of the strict energetic requirement $E_S \approx 2 E_T$.¹¹ Linear acenes and their derivatives are by far the most studied organic semiconductors for SF and there is a correlation between the number of benzene units and the singlet-triplet energy gap. For instance, SF is endergonic for tetracene and exergonic for pentacene.¹²⁻¹⁴ Several models have been designed to investigate the SF kinetics in solid-state systems¹⁵⁻¹⁷, and many attempts at experimentally resolving the kinetic parameters using EPR spectroscopy have been reported.^{9,10,18,19} Nonetheless, several key points remain under discussion, such as the extent of triplet correlation after the initial SF event.⁷ Recent studies have explored the effect of diffusion on the kinetics revealing that it plays a significant role in the successful dissociation of excitons into free triplets.^{20,21} A study by Broch et al.²² observed that the rate of SF in pentacene crystalline films was unaffected by dilution on early timescales accessible from optical spectroscopy. It was proposed that diffusion to hot spots was the key to the invariance in rate constants. Although both the measurement techniques and the nature of the molecular host matrix were different to the system presented here, similar structural and optical properties were observed.^{10,23} Therefore, we can assume that the kinetics of our dilute system represent the behaviour of a dense film.

Numerous studies have shown that relative molecular orientation plays a role in inter-chromophore coupling and the efficiency of SF. The slip-stacked geometry is commonly identified as most favourable for singlet fission,^{12,23,24} but theoretical studies suggest that herringbone packing could also be suitable.²⁵ The exciton delocalisation on non-covalent dimers has been

studied,^{26–30} but the effect of molecular configurations on SF dynamics is not explicitly addressed. Structural considerations and dilution of acene molecules on the inter-triplet interactions have been considered, but the measurements could not distinguish between herringbone or slip-stacked.^{22,31} Several theoretical studies compare molecular systems with stacked or herringbone motifs in their crystal packing, addressing the effect of the relative orientation between neighbouring chromophores on the spin and thermodynamics of SF and subsequent exciton migration,^{32–35} but to our knowledge no such study has been reported experimentally in solid-state crystalline systems. Calculations have predicted that the optimal geometry for SF is that which results in a substantial orbital overlap for both HOMO and LUMO, however this has been attributed to both herringbone and slip-stacked configurations.^{12,30,32–35} Therefore, a combined experimental and theoretical methodology that allows to isolate and distinguish the kinetics of herringbone and slip-stacked dimers in the SF process would be a valuable addition to the field.

More recently, a comprehensive modelling of ethylene pairs showed that the slip-stacked arrangement is one of the most efficient geometries for SF in terms of exciton harvesting.³⁵ Consequently, covalent dimers of perylene-3,4,9,10-bis(dicarboximide) (PDI) and terrylene-3,4,11,12-bis(dicarboximide) (TDI) with slip-stacked geometries have been synthesised and identified as efficient SF materials in solution *via* EPR spectroscopy.^{36–38} A recent study on these same materials found faster dynamics in the ordered slip-stacked TDI film than in the randomly ordered PDI.³⁹ Previous work suggests that the dimer configuration affects the efficiency of quintet dissociation and therefore the potential for triplet harvesting within these layers.¹⁰ Specifically, the ⁵(TT) states from parallel and herringbone dimers have distinct Hamiltonian parameters and the coupled triplets originating from parallel dimers dissociate more readily. This

work aims to expand on these findings by performing a complete study of the kinetic and thermodynamic parameters.

Here we explore the effect of the relative molecular orientation on the energy landscape of a well-defined pentacene system.⁴⁰ We investigate the dissociation kinetics in a dilute system where excited state diffusion is likely suppressed. The kinetic parameters are obtained as a function of temperature and pentacene concentration to identify variations in the dynamics of the parallel, specifically slip-stacked, and herringbone configurations. Films of 0.5% and 10% pentacene in *p*-terphenyl are studied, representative of the isolated molecule and partially aggregated systems respectively.⁴⁰ To account for the energetic and kinetic differences found experimentally, we perform density functional theory (DFT) and time dependent DFT (TD-DFT) calculations. These provide the distributed molecular orbitals and strength of electronic coupling between the coupled chromophore pairs, excited state energies and properties, and couplings between the states/orbitals relevant for SF. How the relative molecular orientation affects the thermodynamics of chromophores in the triplet state is a fundamental question with implications not only in SF research but more generally pertaining to the understanding of excited state chromophore-chromophore interactions.

To investigate the excited state dynamics as a function of dimer configuration in solid-state systems, the temperature dependence of the time-resolved (tr) EPR spectra of thin films of pentacene in *p*-terphenyl was considered. Although the singlet fission mechanism itself is temperature independent,⁴¹ the subsequent dissociation into free triplets and recombination to the ground state may be thermally activated depending on the dimer geometry. It is therefore important

to understand how the molecular configurations can affect the generation of excitons, impacting efficiency for potential photovoltaic applications.

A thin film of 0.5% pentacene in *p*-terphenyl, a system of isolated molecules representative of monomer photophysics, was first considered to determine the contribution of triplets generated from intersystem crossing (ISC) as a function of temperature. ISC in pentacene is known to be temperature dependent as it is a vibronic assisted mechanism.^{42,43} The tr-EPR spectra spanning temperatures from 200 K down to 10 K are reported in Figure 1, for the long axis of the pentacene molecule parallel to the magnetic field, with the maximum peak intensity plotted as a function of temperature in the inset. As the temperature decreases, the pentacene triplet intensity decreases linearly, with the yield dropping to a third of its 200 K value after reaching 10 K.

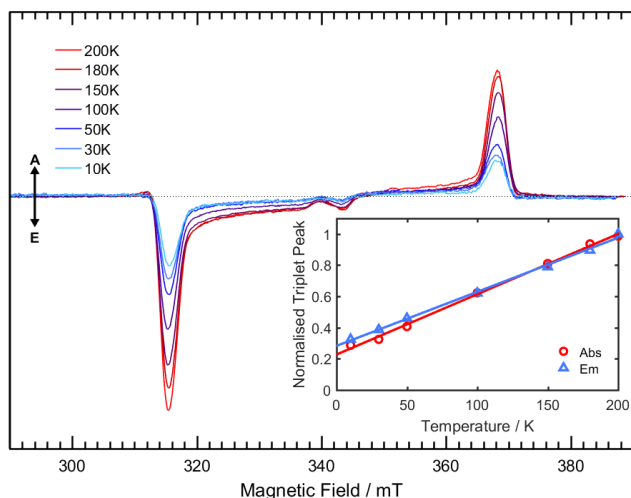


Figure 1. The tr-EPR spectra of the 1 μm thick films of 0.5% pentacene in *p*-terphenyl, integrated over a 500-900 ns time window after the laser pulse. The data are taken as a function of temperature, with the long axis of the molecule aligned with the magnetic field. The maximum intensity for the emission (blue) and absorption (red) peaks are shown in the inset. A = enhanced absorption, E = emission. The feature at ~ 340 mT is attributed to an artefact of the measurement and has been excluded from the kinetic analysis.

The temperature dependence of the tr-EPR spectra of the 10% pentacene film, representative of a partially aggregated system,^{10,40} is shown in Figure 2, measured with the same conditions as the 0.5% film. The spectra are the superposition of three components: isolated triplets from ISC, parallel dimers and herringbone dimers contributing both triplet and quintet species, as reported previously.¹⁰ The triplet to quintet (T/Q) peak ratio for each dimer configuration is reported in the inset as a function of temperature. The expectation would be a constant ratio throughout all measurements due to the temperature independent nature of SF and this is indeed observed for the herringbone dimer (blue dots, Figure 2 inset). In the herringbone geometry, the ratio of triplet to quintet intensities remains constant. Conversely, the T/Q ratio of the parallel dimer geometry decreases with decreasing temperature until 50 K, reaching approximately a quarter of its initial

intensity before settling at a constant ratio. Comparing this with the dilute sample, it can be inferred that the additional triplet contribution at higher temperatures corresponds to the ISC monomer triplet, which then becomes a minor contributor at temperatures below 50 K. . The decrease in T/Q ratio corresponds to the decrease in triplet intensity of the ISC triplet, as measured in the 0.5% pentacene sample.

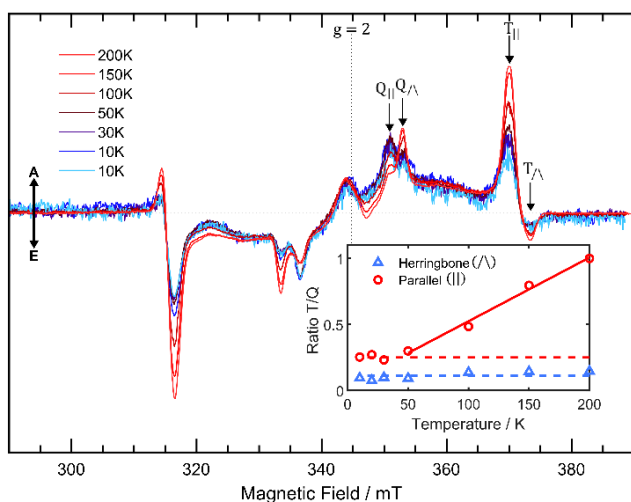


Figure 2. Temperature dependence of the photoexcited EPR spectra of 10% pentacene in p-terphenyl with the long axis of the molecule parallel to the magnetic field. Inset shows the peak intensity ratios of the triplet and quintet peaks for herringbone and parallel dimer configurations as a function of temperature. A = enhanced absorption, E = emission.

To understand the temperature dependence of these phenomena, we analyse the dynamics according to the Arrhenius equation which relates the rate constant, k , of a reaction to temperature *via*:

$$k = A \exp\left(-\frac{E_a}{k_B T}\right) \quad (2)$$

where A is a prefactor, E_a is the activation energy, k_B is the Boltzmann constant and T is temperature.

The decay rates of the ISC triplets back to the ground state for the 0.5% pentacene sample were calculated at each temperature and an Arrhenius plot reported in the supporting information. As the temperature is lowered below ~ 190 K, *p*-terphenyl undergoes a phase change from a monoclinic to triclinic structure, allowing pentacene to substitute into four inequivalent sites instead of just two.^{44,45} Most noticeably, the pentacene reordering results in a 20% decrease of the decay rate when lowering the temperature through the structural phase transition (see supporting information Figure S2). This effect has not previously been reported, as this is the first time an EPR study has included the phase transition temperature of *p*-terphenyl. However, it could be significant in predicting optimal crystal structures for optically active materials. The remaining data below 190 K then follow the exponential increase in lifetime with decreasing temperature.

The temperature-dependent kinetics were calculated for the 10% pentacene sample solving a set of ordinary differential rate equations, similar to those used previously for pentacene in *p*-terphenyl system^{13,46} but modified to include both dimer configurations and independent ISC generated triplets simultaneously:

$$\dot{Q}_{\wedge} = k_{TQ_{\wedge}}TT_{\wedge} - (k_{diss_{\wedge}} + k_{Qrec_{\wedge}})Q_{\wedge} + \text{ratio}Q_0 * k_{irf} * S_1 \quad (3a)$$

$$\dot{TT}_{\wedge} = -k_{TQ_{\wedge}}TT_{\wedge} + k_{diss_{\wedge}}Q_{\wedge} - k_{diff_{\wedge}}TT_{\wedge} - k_{TTrec_{\wedge}}TT_{\wedge} \quad (3b)$$

$$\dot{Q}_{\parallel} = k_{TQ_{\parallel}}TT_{\parallel} - (k_{diss_{\parallel}} + k_{Qrec_{\parallel}})Q_{\parallel} + \text{ratio}Q_0 * k_{irf} * S_1 \quad (3c)$$

$$\dot{TT}_{\parallel} = -k_{TQ_{\parallel}}TT_{\parallel} + k_{diss_{\parallel}}Q_{\parallel} - k_{diff_{\parallel}}TT_{\parallel} - k_{TTrec_{\parallel}}TT_{\parallel} \quad (3d)$$

$$\dot{T} = k_{diff\parallel}TT_{\parallel} + k_{diff\wedge}TT_{\wedge} - k_{Trec}T + \text{ratio}T_0 * k_{irf} * S_1 \quad (3e)$$

$$\dot{S}_0 = k_{Trec}T + k_{TTrec\parallel}TT_{\parallel} + k_{Qrec\parallel}Q_{\parallel} + k_{Qrec\wedge}Q_{\wedge} + k_{TTrec\wedge}TT_{\wedge} \quad (3f)$$

$$\dot{S}_1 = -k_{irf} * S_1 \quad (3g)$$

Here, Q and TT are the density of quintet and dissociated triplets for the parallel, denoted by \parallel , and herringbone, denoted by \wedge , cases; T , S_0 and S_1 are the monomer triplet, ground state and excited singlet state densities, respectively. The population at time zero is assumed to be entirely in S_1 , which then evolves into independent triplets or either variety of quintet according to ratios, namely ratio T_0 and ratio Q_0 that are fitted to the experimental data. We assume that the ratio of quintets formed is independent of the dimer geometry.

The kinetic parameters are the rate of dissociation:

$$k_{diss} = {}^5(TT) \rightarrow T + T \quad (4)$$

the rate of diffusion:

$$k_{diff} = T + T \rightarrow 2T \quad (5)$$

the rate of back-transfer from triplets to quintet:

$$k_{TQ} = T + T \rightarrow {}^5(TT) \quad (6)$$

the triplets' decay:

$$k_{Trec} = T \rightarrow S_0 \quad (7)$$

$$k_{TTrec} = T + T \rightarrow S_0 + S_0 \quad (8)$$

and the quintet recombination to ground state:

$$k_{Qrec} = {}^5(TT) \rightarrow S_0S_0 \quad (9)$$

with the corresponding configuration subscript, || or \wedge , where relevant. The fitted data are shown in Figure 3 along with a schematic of the kinetic model. As the spectral features corresponding to the parallel dimer triplet contribution consist of overlapping SF generated triplets and monomer triplets generated by ISC, the kinetic model includes both pathways and treats them independently. The triplet populations due to SF and ISC mechanisms are summed to generate a full kinetic spectrum. As the ISC contribution is temperature dependent, the proportion of ISC triplet is fitted at each temperature, though it was found to return a constant ratio below 50 K. Given that the proposed model considers all possible dynamic processes at once, including the coupling between parallel and herringbone configurations, it requires a total of 11 rate constants at each temperature, which can be simplified to 9, as detailed below. Including the activation energies to model all temperatures simultaneously and the initial ratio of quintet at 200 K increases this number to 19 parameters to model the entire temperature dependent dataset. To constrain the values to lie within physically reasonable bounds, we limit activation energies to 5 meV. The processes are interlinked as dictated by the ordinary differential equations 3(a-g) and are thermally activated. Moreover, the simulation is defined as a global fit over all temperatures. This approach minimises the number of fitting parameters needed, however, discrepancies between experimental and simulated traces are expected. Individual fits achieved with fewer constraints and more fitting parameters can provide better agreement but may not be physically meaningful.

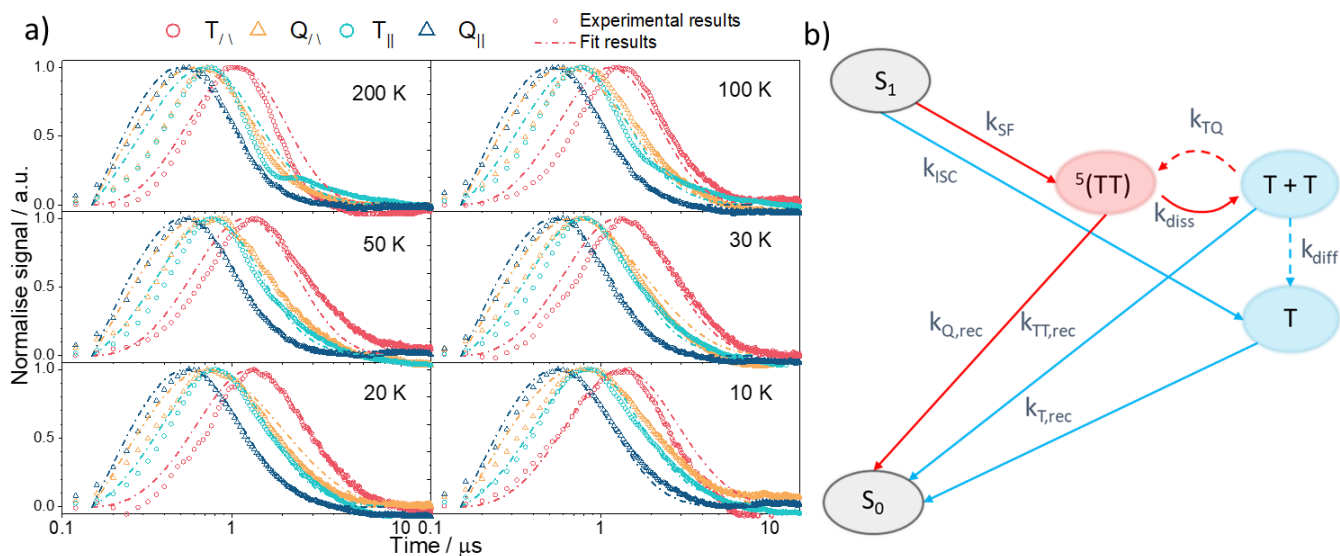


Figure 3. a) Photoexcited Tr-EPR spectra of 10% pentacene in p-terphenyl measured with the molecule's long axis parallel to the magnetic field (open circles) and corresponding fits from the 9-parameter kinetic model (dashed lines). The 4 signal decays are from the herringbone triplets (red) and quintets (yellow) and parallel triplets (green) and quintets (blue). The different panels show the decay at different temperatures from 200 K to 10 K. b) Diagram illustrating the kinetic rate constants described by the differential equations given in the main text. The black, red and blue bubbles are the singlet quintet and triplet states respectively. The dotted lines represent the rate constants that are deemed negligible in this system.

Applying this model, it was found that several simplifications of the rate equations were possible: (1) The activation energy was negligible in most rate constants confirming that SF is temperature independent. The quintet recombination to the ground state is the only exception, reaching the upper limit of the set boundary, indicating an energetically unfavourable transition. (2) The diffusion term proved to be unnecessary to explain the data. Previous structural work demonstrated that pentacene aggregates at 10% concentration could not be larger than crystal size

that can be detected by XRD, namely 5 nm.^{10,40} The lack of diffusion suggests the films are homogeneously blended at the molecular level, with aggregates of pentacene mostly limited to dimers in the 10% films. (3) The rate constants of back-transfer from triplets to quintets, k_{TQ} , were also found to be negligible irrespective of the dimer configuration. This is unsurprising considering the overall downhill energy landscape of singlet fission in pentacene. Quintet dissociation, k_{diss} , is 2.5 times faster in the parallel dimer, as previously reported,¹⁰ but now it is found that the triplet pair recombination, k_{TTrec} , to the ground state is also faster in the parallel dimer by a factor of 2. The kinetic parameters are given in Figure S3 and Table S1.

To aid our understanding of the differing dynamics of the two dimer configurations, DFT calculations were performed. As the crystal structure of the *p*-terphenyl: pentacene blends has yet to be determined, the crystal structure of pure pentacene was used to optimise the dimers, although we caution that there may be slight variations in the herringbone angle of the dimers from dilution in the *p*-terphenyl matrix. From the pentacene crystal structure four inequivalent pairs of molecules are identified. These are the herringbone pair (HB), the slip-stacked parallel pair along the *a* cell axis (SS), the cofacial parallel along the *b* cell axis (CP) and the head-to-tail parallel along the *c* cell axis (HT), reported in Figure S4, with the shortest distances between carbon atoms labelled. In the same figure we include the calculated hole and electron transfer integrals for all three parallel dimers and the herringbone dimer.

EPR spectroscopy does not differentiate between the different parallel configurations as pairs are defined by the intermolecular angle, which is the same for all parallel configurations, however in DFT each pair is considered separately. Some of the dimers are not relevant and can be excluded from further consideration. For example, only molecules with nearest neighbour separations up to 4 Å have sufficiently strong intermolecular interactions from the π - π stacking to undergo

delocalisation of the electronic states.⁴⁷⁻⁴⁹ The CP dimer can therefore be excluded as participating in SF as the intermolecular separation is too large resulting in couplings only on the order of μeV . Similarly, the transfer integrals of the HT configuration are orders of magnitude weaker than for the HB and SS configurations, therefore only the latter are compared here. These calculations indicate that the parallel pair observed experimentally is most likely a SS dimer. Hence, here we focus only on HB and SS dimers.

The frontier molecular orbitals calculated for the HB and SS geometries are shown in Figure 4 (with additional orbitals shown in Figures S5-8). The calculations show that in the herringbone geometry the orbitals are localised on one or the other molecule, whereas in the parallel geometries these are delocalised over both. This result suggests that excitons in the HB can have either charge-transfer character (where positive and negative charge in the exciton are spatially separated) or Frenkel character whereas excitons in the SS configuration would only have Frenkel character, although they would be delocalized over two units.

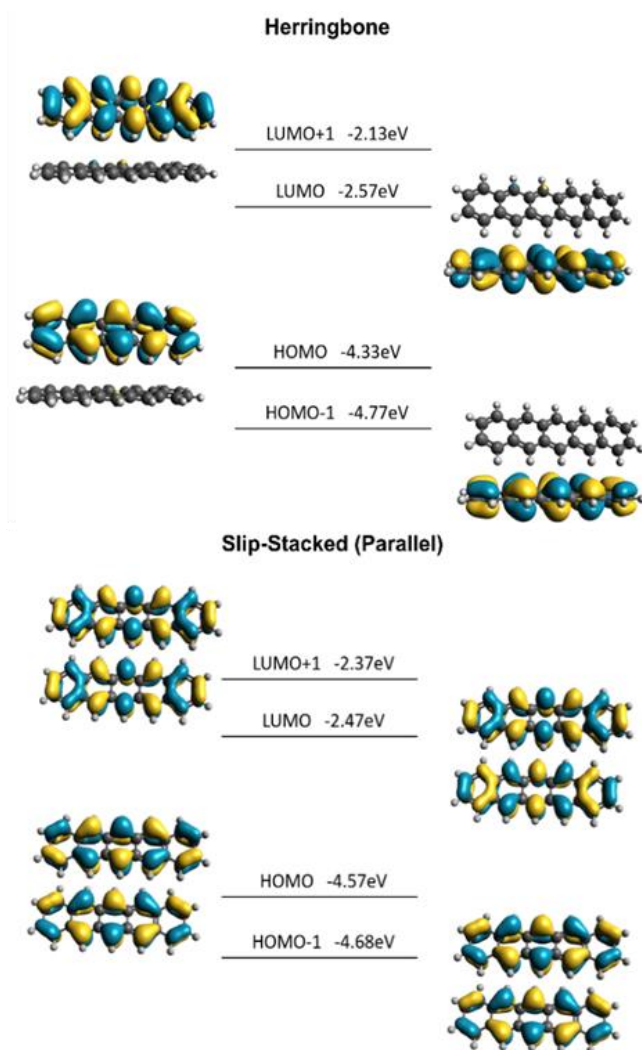


Figure 4. Calculated molecular orbitals for the pentacene monomer and the three dimer configurations that participate in SF: herringbone, slip-stacked and head-to-tail parallel.

Table 1. Excited states calculated using TD-DFT (B3LYP/6-31g(d,p)) for the pentacene monomer, herringbone dimer and parallel dimer. Character of each state was determined based on participating orbital transitions and confirmed by calculated charge distribution (presented in SI). In the last column spin-orbit coupling for the triplet to ground state interaction.

	Energy (eV)	Oscillator Strength	Character	$\langle S_0 \text{SOC} T_n \rangle$ (cm^{-1})
--	-------------	---------------------	-----------	---

MONOMER				
T ₁	0.60	0	-	0.000
T ₂	1.89	0	-	0.696
S ₁	1.91	0.0412	-	-
HERRINGBONE DIMER				
T ₁	0.56	0	F	0.100
T ₂	0.59	0	F	0.379
S ₁	1.31	0.0071	CT	-
T ₃	1.32	0	CT	0.337
T ₄	1.87	0	F	1.059
T ₅	1.89	0	F	0.527
S ₂	1.91	0.0492	F	-
S ₃	1.93	0.0258	F	-
SLIP-STACKED DIMER				
T ₁	0.58	0	Frenkel	0.000
T ₂	0.59	0		0.221
S ₁	1.75	0.0527		-
T ₃	1.79	0		0.302
S ₂	1.79	0		-
T ₄	1.80	0		0.000
T ₅	1.88	0		1.086
T ₆	1.89	0		0.000
S ₃	1.95	0		-
S ₄	1.97	0.0575		0.000

TD-DFT calculations of excited state energies and charge distributions confirmed those predictions. Energies and oscillator strengths of the excited states for the pentacene monomer and the two dimers, HB and SS, are presented in Table 1; charge distributions for the excited states are presented in Supplementary Tables S4-6. The excited state energies are sensitive to the DFT functional used. Thus, to choose the best method we selected the functional which gave the best agreement with the experimental absorption spectrum of the pentacene monomer, namely B3LYP/6-31g(d,p).¹⁰ The calculated singlet energies are in relatively good agreement with those

obtained experimentally.¹⁰ The two lowest triplet energies are close for both dimers and nearly identical to the monomer, even though they are lower than experimental values.⁵⁰ The differences between calculated and experimental triplet energies are expected due to limitations in TD-DFT in accurately predicting energies for large molecules.⁵¹ The calculated excited state structure in the HB dimer reveals both triplet and singlet states of CT character at relatively low energy. In contrast, the excited states of the SS dimer are delocalised over both monomers, as would be expected from the symmetry of the SS dimer orbitals. The optoelectronic processes in the HB dimer are therefore more likely to be CT mediated than those occurring in the SS dimer. We treat the TDDFT calculations more qualitatively, as the energies, especially of CT states, are often underestimated and depend on the method used. However, we reproduced the CT character of the states and the orbital separation of the HB dimers using other functionals.

The quintet dissociation process is usually connected to spin coupling between triplets, while the electronic coupling is neglected. Quintet dissociation and other SF processes involve doubly excited states, however calculations of those states and the transition rate constant between them are computationally expensive.¹⁸ Instead we propose a simpler method whereby calculations of transition dipole moments (tdm) between relevant singly excited states, specifically low energy triplets, can yield information about the couplings between them and enable correlation of couplings with the dissociation and recombination rate constants in the two dimer structures. We calculated relevant tdm using the PySOC code implemented to Gaussian output.⁵²

First, we compare the calculated tdm between the two lowest energy triplets T_1 and T_2 in both dimers (Table 2). We assume that the quintet and correlated triplet pair formed in pentacene are mainly composed of the T_1 and T_2 triplet states calculated in the dimer structures. T_1 and T_2 triplet states originate from two T_1 triplet state for two monomers, thus we can also assume that T_1+T_2

correlated triplet pair splits into two T_1 states localized on single pentacene molecules. According to the generalized Mulliken-Hush theory, we propose that tdm between T_1 and T_2 reflects the strength of the electronic coupling between the states.^{53,54}

We propose that tdm between T_1 and T_2 reflects the strength of the electronic coupling between the states. A discussion considering the excited state symmetry is included in the SI. The tdm between T_1 and T_2 for the HB structure, at 9.44 Debye, greatly exceeds the tdm between the same states in SS (0.02 Debye). Since the quintet state observed in SF process is a coupled triplet pair involving these states (T_1T_2), we propose that the stronger coupling between triplets in the HB dimer results in slower quintet dissociation than in the SS dimer. It supports the idea that electronic coupling plays a role in the dissociation process. However, considering that coupling is over two orders of magnitude larger and the dissociation rate only three times lower, it is likely that other interactions also contribute to the kinetics.

Table 2. Comparison between herringbone and slip-stacked dimer of dissociation rate at 200K obtained from the kinetic model and calculated transition dipole moment between triplets T₁ and T₂.

	HERRING-BONE	SLIP-STACKED
Quintet dissociation rate, k_{diss} , at 200K (kinetic model)	0.6 μs^{-1}	1.58 μs^{-1}
Transition dipole moment $\langle T_1 r T_2 \rangle$	9.44 Debye	0.02 Debye
Triplet pair recombination rate, $k_{\text{TT, rec}}$, at 200K (kinetic model)	3.88 μs^{-1}	7.5 μs^{-1}
Sum of spin-orbit coupling between T _n (n=1,2) and ground state : $\langle S_0 \text{SOC} T_1 \rangle + \langle S_0 \text{SOC} T_2 \rangle$	0.479 cm^{-1}	0.221 cm^{-1}

To seek an explanation for the different rate constants of recombination of correlated triplet pairs to the ground state, where the rate constant is around two times higher in SS than in HB dimer, we compare calculated spin-orbit couplings of the triplets involved, T₁ and T₂, to the ground state. The calculated couplings show the opposite trend to the observed rate constants (Table 2). However, the calculations relate to individual triplets rather than correlated pairs, and the nature of correlated triplet pair is not yet well understood. Knowing that the rate constants of triplet recombination and

correlated triplet pair recombination are different, we propose that the recombination dynamics of correlated triplet pair depend on factors other than the spin-orbit coupling to the ground state. Since the correlated triplets cannot be treated separately, the recombination rate can also be determined by the strength of the coupling between the triplets. Thus, the recombination rate for correlated triplets could be the interplay between the coupling to the ground and interaction between the triplets.

The comparison between calculated interactions for excited states involved in the singlet fission process in HB and SS dimer structures provide an insight into the dynamics of SF processes, like quintet dissociation or triplet pair recombination. We show that strong electronic coupling between triplets in the HB structure can be the reason for slow dissociation and slow triplet pair recombination.

Our study details the effects of molecular orientation on the kinetics of the SF mechanism. This is of particular relevance as hybrid devices are being successfully engineered but still require significant optimisation,⁶ which we postulate can be achieved through control of intermolecular geometries. The systematic study of triplet and quintet species in dilute pentacene films, achieved using EPR spectroscopy at cryogenic temperatures, has enabled the ISC and SF contributions to be distinguished and quantified. The results demonstrate how a slight change in the relative molecular orientation impacts the kinetics and could therefore be used to predict optimal crystal structures for SF. Exploiting the unique ability of EPR to distinguish between molecular configurations of paramagnetic species, the kinetic parameters for both dimer geometries were modelled simultaneously. Most processes required no thermal activation and there was no evidence of diffusion of triplets away from correlated triplet pairs. This is indicative of a homogenous dilute blend where pentacene is dispersed in the matrix at the scale of single

molecules and pairs. As previously reported, dissociation was found to be more efficient in parallel dimers, and DFT calculations provided an insight into why this is so. It was found that the electronic coupling between dissociated triplets was weaker in the parallel configurations with orbitals delocalised over both molecules. Conversely, the herringbone dimer has orbitals localised on one molecule or the other, resulting in excited states with charge transfer character, and high electronic coupling between triplets, which leads to inefficient dissociation. Our results demonstrate the important role of electronic coupling in the dynamics of SF materials and its correlation to molecular configuration. While the generation of charges from SF for solar cell applications involves multiple processes and recent work has highlighted that the generation of charges from triplets is surprisingly slow,⁵⁵ our findings provide guidelines for optimising free triplet generation, which is a crucial step in photovoltaic operation.

ASSOCIATED CONTENT

Supporting Information. Experimental details; isolated molecule information and data; complete DFT results and molecular orbital diagrams.

This material is available free of charge via the Internet at <http://pubs.acs.org>.

AUTHOR INFORMATION

Corresponding Author

* Professor Sandrine Heutz (s.heutz@imperial.ac.uk), Dr Daphné Lubert-Perquel (d.lubert-perquel@magnet.fsu.edu), Professor Jenny Nelson (jenny.nelson@imperial.ac.uk) and Dr Enrico Salvadori (enrico.salvadori@unito.it).

Present Addresses

† National High Magnetic Field Laboratory, 1800 E Paul Dirac Dr, Tallahassee, FL 32310.

Notes

The authors declare no competing financial interests.

ACKNOWLEDGMENT

D.L.P. acknowledges a studentship from the UK Engineering and Physical Sciences Research Council (EPSRC) Centre for Doctoral Training for the Advanced Characterisation of Materials (EP/L015277/1). S.R. and C.W.M.K. acknowledge financial support from the University of Saarland. A.A.Sz. acknowledges a studentship from the European Research Council (ERC) Synergy Program (grant no. 610115). J.N., M.A. and A.A.Sz. acknowledge financial support from the ERC (Advanced Grant, action no. 742708) and from the EPSRC (EP/P005543/1).

REFERENCES

- (1) Zhang, J. P.; Inaba, T.; Watanabe, Y.; Koyama, Y. Partition of Carotenoid-to-Bacteriochlorophyll Singlet-Energy Transfer through Two Channels in the LH2 Complex from *Rhodobacter Sphaeroides* G1C. *Chem. Phys. Lett.* **2001**, *340*, 484.
- (2) Polli, D.; Cerullo, G.; Lanzani, G.; De Silvestri, S.; Hashimoto, H.; Cogdell, R. J. Carotenoid-Bacteriochlorophyll Energy Transfer in LH2 Complexes Studied with 10-Fs Time Resolution. *Biophys. J.* **2006**, *90*, 2486.
- (3) Tabernig, S. W.; Daiber, B.; Wang, T.; Ehrler, B. Enhancing Silicon Solar Cells with Singlet Fission: The Case for Förster Resonant Energy Transfer Using a Quantum Dot Intermediate. *J. Photonics Energy* **2018**, *8* (02), 1.
- (4) MacQueen, R.; Liebhaber, M.; Niederhausen, J.; Mews, M.; Gersmann, C.; Jäckle, S.; Jäger,

- K.; Tayebjee, M. J. Y.; Schmidt, T. W.; Rech, B.; et al. Crystalline Silicon Solar Cells with Tetracene Interlayers: The Path to Silicon-Singlet Fission Heterojunction Devices. *Mater. Horizons* **2018**, *5*, 1065.
- (5) Davis, N. J. L. K.; Allardice, J. R.; Xiao, J.; Petty, A. J.; Greenham, N. C.; Anthony, J. E.; Rao, A. Singlet Fission and Triplet Transfer to PbS Quantum Dots in TIPS- Tetracene Carboxylic Acid Ligands. *J. Phys. Chem. Lett.* **2018**, *9*, 1454–1460.
- (6) Einzinger, M.; Wu, T.; Kompalla, J. F.; Smith, H. L.; Perkinson, C. F.; Nienhaus, L.; Wieghold, S.; Congreve, D. N.; Kahn, A.; Bawendi, M. G.; et al. Sensitization of Silicon by Singlet Exciton Fission in Tetracene. *Nature* **2019**, *571* (7763), 90–94.
- (7) Musser, A. J.; Clark, J. Triplet-Pair States in Organic Semiconductors. *Annu. Rev. Phys. Chem.* **2019**, *70*, 323.
- (8) Tayebjee, M. J. Y.; Sanders, S. N.; Kumarasamy, E.; Campos, L. M.; Sfeir, M. Y.; McCamey, D. R. Quintet Multiexciton Dynamics in Singlet Fission. *Nat. Phys.* **2017**, *13* (2), 182–188.
- (9) Weiss, L. R.; Bayliss, S. L.; Kraffert, F.; Thorley, K. J.; Anthony, J. E.; Bittl, R.; Friend, R. H.; Rao, A.; Greenham, N. C.; Behrends, J. Strongly Exchange-Coupled Triplet Pairs in an Organic Semiconductor. *Nat. Phys.* **2017**, *13* (October), 176–181.
- (10) Lubert-Perquel, D.; Salvadori, E.; Dyson, M.; Stavrinou, P. N.; Montis, R.; Nagashima, H.; Kobori, Y.; Heutz, S.; Kay, C. W. M. Identifying Triplet Pathways in Dilute Pentacene Films. *Nat. Commun.* **2018**, *9*, 4222.

- (11) Fallon, K. J.; Budden, P.; Salvadori, E.; Ganose, A. M.; Savory, C. N.; Eyre, L.; Dowland, S.; Ai, Q.; Goodlett, S.; Risko, C.; et al. Exploiting Excited-State Aromaticity to Design Highly Stable Singlet Fission Materials. *J. Am. Chem. Soc.* **2019**, *141* (35), 13867–13876.
- (12) Smith, M. B.; Michl, J. Recent Advances in Singlet Fission. *Annu. Rev. Phys. Chem.* **2013**, *64*, 361–386.
- (13) Dover, C. B.; Gallaher, J. K.; Frazer, L.; Tapping, P. C.; Petty, A. J.; Crossley, M. J.; Anthony, J. E.; Kee, T. W.; Schmidt, T. W. Endothermic Singlet Fission Is Hindered by Excimer Formation. *Nat. Chem.* **2018**, *10* (3), 305–310.
- (14) Stern, H. L.; Musser, A. J.; Gelinas, S.; Parkinson, P.; Herz, L. M.; Bruzek, M. J.; Anthony, J.; Friend, R. H.; Walker, B. J. Identification of a Triplet Pair Intermediate in Singlet Exciton Fission in Solution. *Proc. Natl. Acad. Sci.* **2015**, *112* (25), 7656–7661.
- (15) Merrifield, R. E. Magnetic Effects on Triplet Exciton Interactions. *Pure Appl. Chem.* **1971**, *27* (3), 481–498.
- (16) Yago, T.; Ishikawa, K.; Katoh, R.; Wakasa, M. Magnetic Field Effects on Triplet Pair Generated by Singlet Fission in an Organic Crystal: Application of Radical Pair Model to Triplet Pair. *J. Phys. Chem. C* **2016**, *120* (49), 27858–27870.
- (17) Yost, S. R.; Lee, J.; Wilson, M. W. B.; Wu, T.; McMahon, D. P.; Parkhurst, R. R.; Thompson, N. J.; Congreve, D. N.; Rao, A.; Johnson, K.; et al. A Transferable Model for Singlet-Fission Kinetics. *Nat. Chem.* **2014**, *6* (6), 492–497.
- (18) Basel, B. S.; Zirzmeier, J.; Hetzer, C.; Phelan, B. T.; Krzyaniak, M. D.; Reddy, S. R.; Coto,

- P. B.; Horwitz, N. E.; Young, R. M.; White, F. J.; et al. Unified Model for Singlet Fission within a Non-Conjugated Covalent Pentacene Dimer. *Nat. Commun.* **2017**, *8* (May), 15171.
- (19) Tayebjee, M. J. Y.; Sanders, S. N.; Kumarasamy, E.; Campos, L. M.; Sfeir, M. Y.; McCamey, D. R. Quintet Multiexciton Dynamics in Singlet Fission. *Nat. Phys.* **2017**, *13* (2), 182–188.
- (20) Shushin, A. I. Kinetics of Singlet Fission in Organic Semiconductors: Specific Features of T-Exciton Migration Effects. *J. Chem. Phys.* **2019**, *151* (3).
- (21) Lee, T. S.; Lin, Y. L.; Kim, H.; Rand, B. P.; Scholes, G. D. Two Temperature Regimes of Triplet Transfer in the Dissociation of the Correlated Triplet Pair after Singlet Fission. *Can. J. Chem.* **2019**, *97* (6), 465–473.
- (22) Broch, K.; Dieterle, J.; Branchi, F.; Hestand, N. J.; Olivier, Y.; Tamura, H.; Cruz, C.; Nichols, V. M.; Hinderhofer, A.; Beljonne, D.; et al. Robust Singlet Fission in Pentacene Thin Films with Tuned Charge Transfer Interactions. *Nat. Commun.* **2018**, *9* (1), 954.
- (23) Kolata, K.; Breuer, T.; Witte, G.; Chatterjee, S. Molecular Packing Determines Singlet Exciton Fission in Organic Semiconductors. *ACS Nano* **2014**, *8* (7), 7377–7383.
- (24) Felter, K. M.; Grozema, F. C. Singlet Fission in Crystalline Organic Materials: Recent Insights and Future Directions. **2019**.
- (25) Feng, X.; Kolomeisky, A. B.; Krylov, A. I. Dissecting the Effect of Morphology on the Rates of Singlet Fission: Insights from Theory. *J. Phys. Chem. C* **2014**, *118* (34), 19608–19617.

- (26) Zimmerman, P. M.; Bell, F.; Casanova, D.; Head-Gordon, M. Mechanism for Singlet Fission in Pentacene and Tetracene : From Single Exciton to Two Triplets. *J. Am. Chem. Soc.* **2011**, *133*, 19944–19952.
- (27) Tamura, H.; Huix-rotllant, M.; Burghardt, I.; Olivier, Y.; Beljonne, D. First-Principles Quantum Dynamics of Singlet Fission : Coherent versus Thermally Activated Mechanisms Governed by Molecular π Stacking. *Phys. Rev. Lett.* **2015**, *115*, 107401.
- (28) Monahan, N. R.; Sun, D.; Tamura, H.; Williams, K. W.; Xu, B.; Zhong, Y.; Kumar, B.; Nuckolls, C.; Harutyunyan, A. R.; Chen, G.; et al. Dynamics of the Triplet-Pair State Reveals the Likely Coexistence of Coherent and Incoherent Singlet Fission in Crystalline Hexacene. *Nat. Chem.* **2016**, *9* (4), 341–346.
- (29) Sutton, C.; Tummala, N. R.; Beljonne, D.; Bredas, J. L. Singlet Fission in Rubrene Derivatives : Impact of Molecular Packing. *Chem. Mater.* **2017**, *29*, 2777–2787.
- (30) Okada, K.; Tonami, T.; Nagami, T.; Nakano, M. Breakdown of the Perturbative Approach to Molecular Packing Dependence of Singlet Fission Rates in Pentacene Dimer Models : A Systematic Comparison with the Quantum Master Equation Approach. *J. Phys. Chem. C* **2019**, *123*, 15403–15411.
- (31) Yong, C. K.; Musser, A. J.; Bayliss, S. L.; Lukman, S.; Tamura, H.; Bubnova, O.; Hallani, R. K.; Meneau, A.; Resel, R.; Maruyama, M.; et al. The Entangled Triplet Pair State in Acene and Heteroacene Materials. *Nat. Commun.* **2017**, *8* (May), 15953.
- (32) Buchanan, E. A.; Michl, J. Packing Guidelines for Optimizing Singlet Fission Matrix Elements in Noncovalent Dimers. *J. Am. Chem. Soc.* **2017**, *139* (44), 15572–15575.

- (33) Wang, X.; Liu, X.; Tom, R.; Cook, C.; Schatschneider, B. Phenylated Acene Derivatives as Candidates for Intermolecular Singlet Fission. *J. Phys. Chem. C* **2019**, *123*, 5890–5899.
- (34) Tao, G. Nonadiabatic Simulation of Singlet Fission Dynamics in Tetracene Clusters: The Topology of Quantum Coherence in a Global View. *J. Chem. Phys.* **2019**, *151* (5).
- (35) Zaykov, A.; Felkel, P.; Buchanan, E. A.; Jovanovic, M.; Havenith, R. W. A.; Kathir, R. K.; Broer, R.; Havlas, Z.; Michl, J. Singlet Fission Rate: Optimized Packing of a Molecular Pair. Ethylene as a Model. *J. Am. Chem. Soc.* **2019**.
- (36) Margulies, E. A.; Shoer, L. E.; Eaton, S. W.; Wasielewski, M. R. Excimer Formation in Cofacial and Slip-Stacked Perylene-3,4:9,10-Bis(Dicarboximide) Dimers on a Redox-Inactive Triptycene Scaffold. *Phys. Chem. Chem. Phys.* **2014**, *16*, 23735–23742.
- (37) Chen, M.; Bae, Y. J.; Mauck, C. M.; Mandal, A.; Young, R. M.; Wasielewski, M. R. Singlet Fission in Covalent Terrylenediimide Dimers: Probing the Nature of the Multiexciton State Using Femtosecond Mid-Infrared Spectroscopy. *J. Am. Chem. Soc.* **2018**, *140*, 9184–9192.
- (38) Mandal, A.; Chen, M.; Foszcz, E. D.; Schultz, J. D.; Kearns, N. M.; Young, R. M.; Zanni, M. T.; Wasielewski, M. R. Two-Dimensional Electronic Spectroscopy Reveals Excitation Energy-Dependent State Mixing during Singlet Fission in a Terrylenediimide Dimer. *J. Am. Chem. Soc.* **2018**, *140*, 17907–17914.
- (39) Bae, Y. J.; Zhao, X.; Kryzaniak, M. D.; Nagashima, H.; Strzalka, J.; Zhang, Q.; Wasielewski, M. R. Spin Dynamics of Quintet and Triplet States Resulting from Singlet Fission in Oriented Terrylenediimide and Quaterrylenediimide Films. *J. Phys. Chem. C* **2020**, *124* (18), 9822–9833.

- (40) Lubert-Perquel, D.; Kim, D. K.; Robaschik, P.; Kay, C. W. M.; Heutz, S. Growth, Morphology and Structure of Mixed Pentacene Films. *J. Mater. Chem. C* **2019**, *7*, 289–196.
- (41) Stern, H. L.; Cheminal, A.; Yost, S. R.; Broch, K.; Bayliss, S. L.; Chen, K.; Tabachnyk, M.; Thorley, K.; Greenham, N.; Hodgkiss, J. M.; et al. Vibronically Coherent Ultrafast Triplet-Pair Formation and Subsequent Thermally Activated Dissociation Control Efficient Endothermic Singlet Fission. *Nat. Chem.* **2017**, *9* (12), 1205–1212.
- (42) Patterson, F. G.; Lee, H. W. H.; Wilson, W. L.; Fayer, M. D. Intersystem Crossing from Singlet States of Molecular Dimers and Monomers in Mixed Molecular Crystals: Picosecond Stimulated Photon Echo Experiments. *Chem. Phys.* **1984**, *84* (1), 51–60.
- (43) El-Sayed, M. A.; Olmsted III, J. Intersystem Crossing Relative Rates from Pulsed-Excitation Phosphorescence Microwave Double-Resonance. *Chem. Phys. Lett.* **1971**, *11* (5), 568.
- (44) da Costa, A. A. M.; Amado, A. M.; Becucci, M.; Kryschi, C. Order-Disorder Phase Transition in p-Terphenyl and p-Terphenyl:Tetracene Doped Crystals as Studied by Raman Spectroscopy. *J. Mol. Struct.* **1997**, *416*, 69–73.
- (45) Lang, J.; Sloop, D. J.; Lin, T.-S. Dynamics of P-Terphenyl Crystals at the Phase Transition Temperature: A Zero-Field EPR Study of the Photoexcited Triplet State of Pentacene in p-Terphenyl Crystals. *J. Phys. Chem. A* **2007**, *111* (22), 4731–4736.
- (46) Sakai, H.; Inaya, R.; Nagashima, H.; Nakamura, S.; Kobori, Y.; Tkachenko, N. V.; Hasobe, T. Multiexciton Dynamics Depending on Intramolecular Orientations in Pentacene Dimers : Recombination and Dissociation of Correlated Triplet Pairs. *J. Phys. Chem. Lett.* **2018**, *9*,

3354.

- (47) Hestand, N. J.; Spano, F. C. Molecular Aggregate Photophysics beyond the Kasha Model: Novel Design Principles for Organic Materials. *Acc. Chem. Res.* **2017**, *50* (2), 341–350.
- (48) Gisslén, L.; Scholz, R. Crystallochromy of Perylene Pigments: Interference between Frenkel Excitons and Charge-Transfer States. *Phys. Rev. B - Condens. Matter Mater. Phys.* **2009**, *80* (11), 1–23.
- (49) Hoffmann, M.; Soos, Z. G. Optical Absorption Spectra of the Holstein Molecular Crystal for Weak and Intermediate Electronic Coupling. *Phys. Rev. B - Condens. Matter Mater. Phys.* **2002**, *66* (2), 243051–2430518.
- (50) Bakulin, A. a.; Morgan, S. E.; Kehoe, T. B.; Wilson, M. W. B.; Chin, A. W.; Zigmantas, D.; Egorova, D.; Rao, A. Real-Time Observation of Multiexcitonic States in Ultrafast Singlet Fission Using Coherent 2D Electronic Spectroscopy. *Nat. Chem.* **2016**, *8* (January), 16–23.
- (51) Few, S.; Frost, J. M.; Kirkpatrick, J.; Nelson, J. Influence of Chemical Structure on the Charge Transfer State Spectrum of a Polymer:Fullerene Complex. *J. Phys. Chem. C* **2014**, *118* (16), 8253–8261.
- (52) Gao, X.; Bai, S.; Fazzi, D.; Niehaus, T.; Barbatti, M.; Thiel, W. Evaluation of Spin-Orbit Couplings with Linear-Response Time-Dependent Density Functional Methods. *J. Chem. Theory Comput.* **2017**, *13* (2), 515–524.
- (53) Rust, M.; Lappe, J.; Cave, R. J. Multistate Effects in Calculations of the Electronic Coupling

- Element for Electron Transfer Using the Generalized Mulliken-Hush Method. *J. Phys. Chem. A* **2002**, *106* (15), 3930–3940.
- (54) Creutz, C.; Newton, M. D.; Sutin, N. Metal-Ligand and Metal-Metal Coupling Elements. *J. Photochem. Photobiol. A Chem.* **1994**, *82* (1–3), 47–59.
- (55) Pace, N. A.; Korovina, N. V.; Clikeman, T. T.; Holliday, S.; Granger, D. B.; Carroll, G. M.; Nanayakkara, S. U.; Anthony, J. E.; McCulloch, I.; Strauss, S. H.; et al. Slow Charge Transfer from Pentacene Triplet States at the Marcus Optimum. *Nat. Chem.* **2020**, *12* (1), 63–70.
-